ECS Transactions, 35 (6) 199-208 (2011)
10.1149/1.3570862 ©The Electrochemical Society

The Effect of Different Carrier Gases and Channel Thicknesses on the Characteristics of ZnO TFTs Prepared by Atmospheric Pressure Plasma Jet

Kow-Ming Chang[a,b], Sung-Hung Huang[a,*], Chia-Wei Chi[a], Chin-Jyi Wu[c], Je-Wei Lin[c], Chia-Chiang Chang[c]

[a] Department of Electronics Engineering & Institute of Electronics, National Chiao Tung University, 1001 Ta Hsueh Road, Hsinchu, Taiwan 30010, R.O.C.
[b] College of Electrical and Information Engineering, I-Shou University, Kaohsiung County, Taiwan 84001, R.O.C.
[c] Industrial Technology Research Institute, Mechanical and Systems Research Laboratories, 195, Sec. 4, Chung Hsing Rd., Chutung, Hsinchu, Taiwan 31040, R.O.C.

Thin film transistors (TFTs) with a ZnO channel layer deposited by atmospheric pressure plasma jet (APPJ) were demonstrated. ZnO channel layers were fabricated with a non-vacuum and low-temperature process (100°C). The effects of different carrier gases (nitrogen gas and compressed dry air) and channel thickness on the characteristics of ZnO TFTs were investigated. Reactive oxygen species can effectively repair the oxygen vacancies result in a low leakage current. By reducing the channel thickness, the undesired source to drain current flow can be eliminated. By using CDA as a carrier gas and reducing the channel thickness, a subthreshold swing of 3.75 V/decade, a field-effect mobility of 3.49 cm^2/Vs and a Ion/Ioff current ratio of 4.08×10^7 were obtained.

Introduction

Atmospheric pressure plasma technique is used in a variety of material processes including surface modification (1) , etching (2), and thin-film deposition (3, 4). Thin-film deposition process is particularly attractive for industrial applications. Atmospheric pressure plasma technique doesn't need an expensive vacuum chamber and associated pumping system. For manufacturing consideration, it is more suitable for large area applications because of no chamber size limitation. Furthermore, the low-temperature process, high throughput and low cost have high potential in commercial applications.

Amorphous silicon (a-Si) and polysilicon TFTs dominate the active matrix technologies in the flat-panel display industry over the last ten years. However, these silicon-based TFTs have several limitations such as photosensitivity, light degradation, and opacity, etc. Recently, transparent oxide semiconductors have been investigated as an active channel layer. ZnO thin films have attracted much attention due to non-toxic property, low cost, high mobility, and good optical properties (5). Thin films of ZnO can be prepared in a number of ways: pulse laser deposition (6), RF magnetic sputtering (7), metalorganic chemical vapor deposition (8), sol–gel (9), and spray pyrolysis (10). Most of the deposition methods are vacuum system or the high-temperature process. Instead of the conventional vacuum and wet process, atmospheric pressure plasma jet was non-vacuum system and low-temperature process.

For the applications of ZnO TFTs in the flat-panel displays, the off current must be

Downloaded on 2014-04-24 to IP 140.113.38.11 address. Redistribution subject to ECS terms of use (see ecsdl.org/site/terms_use) unless CC License in place (see abstract).

low. Large on-off ratio is preferred when used as switching device. The carrier concentration of un-doped ZnO thin films results from the intrinsic defects. Higher carrier concentration generates the external scattering and unexpected leakage current. As a result, the background electron carrier concentration must be reduced while ZnO was used as a channel layer. Also, to reduce the leakage current of source to drain current flow, thinner channel layer have been proposed by reducing the conductivity of channel layer (11).

In order to reduce the intrinsic defects, the compressed dry air (CDA, ~20% Oxygen gas) was also used as carrier gas to reduce the oxygen vacancies. Next, to improve the performance, the different channel thicknesses were discussed. The purpose of this study is to demonstrate the possibility to fabricate superior performance ZnO TFTs at low temperature by using atmospheric pressure plasma jet. In this work, we integrated ZnO as a channel layer by atmospheric pressure plasma jet and discussed the effects of carrier gases and channel thicknesses on the characteristics of ZnO TFTs.

Experiment

Zinc oxide thin films were grown on the glass substrates as well as high doping silicon substrate by atmospheric pressure plasma jet (APPJ). The high doping silicon wafer was used as gate electrode and thermally grown SiO_2 (110nm) on the silicon substrate was used as gate insulator. Then, ZnO thin films were deposited on SiO_2/Si by APPJ. Figure 1(a) shows a schematic diagram of the experimental apparatus for APPJ. The deposition apparatus mainly is composed of a plasma jet, an ultrasonic generator, and a hot plate. For deposition of ZnO films, zinc nitrate ($Zn(NO_3)_2 \cdot 6H_2O$) dissolved in pure deionized water was used as the precursor. The concentration of zinc nitrate in the D.I. water was 0.2 M. Next, the aqueous solution was ultrasonically atomized at 2.45 MHz into mist and conveyed by carrier gas to the plasma region, which was connected to DC pulse power supply. In order to deposit uniform ZnO thin film for large area, the xy directional scan system was used. The position of plasma jet was fixed and the substrate was on the xy directional scan system. First, start point, end point and the pitch were set. Next, the scan system moved from the start point to the end point through the path shown in Figure 1(b) and the thickness of ZnO films could be controlled by scaning times. The nitrogen (N_2) and compressed dry air (CDA) were used as carrier gases and the thickness of ZnO thin films were kept at 110 nm. The flow rate of both carrier gases was fixed at 300 sccm, while the flow rate of main gas was 35 SLM. The channel thickness was varied from 55nm to 165nm by scan 5 times, 10 times and 15 imes while CDA used as carrier gas. The distance between nozzle and substrate was set as 5 mm. The power and substrate temperature fixed at 630 W and 100°C, respectively. The pattern on ZnO thin film was obtained by conventional photolithography and wet etching using the HCl:H_2O (1:200). Finally, 100nm thick Al source/drain (S/D) layers were patterned by lift-off technique. A schematic cross view of the fabricated TFT is shown in Figure 2.

Downloaded on 2014-04-24 to IP 140.113.38.11 address. Redistribution subject to ECS terms of use (see ecsdl.org/site/terms_use) unless CC License in place (see abstract).

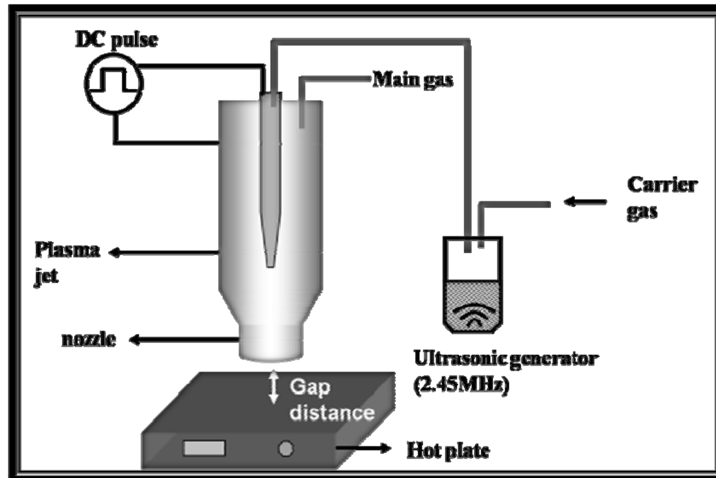

(a)

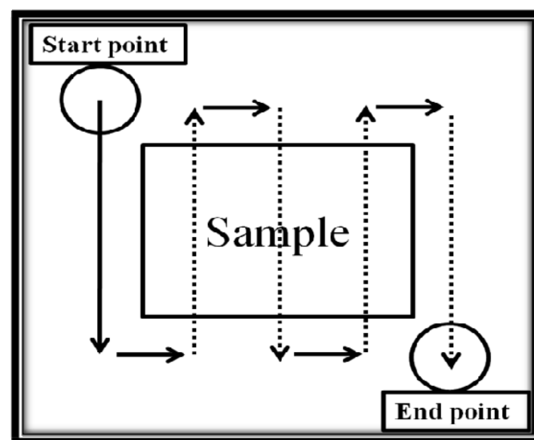

(b)

Figure 1 (a) Schematic diagram of the experimental apparatus (b) Scan path of plasma jet.

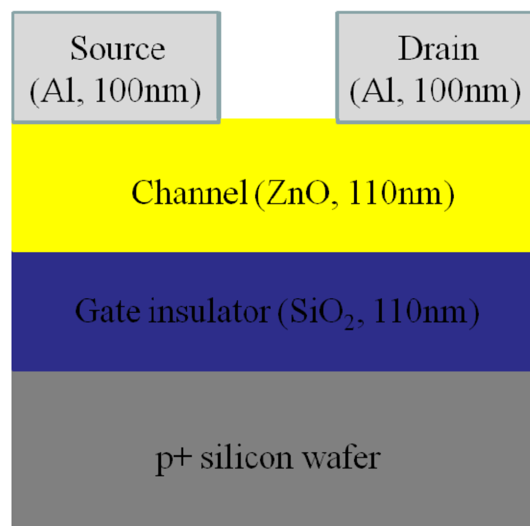

Figure 2 Schematic structure of the bottom-gate TFT test structure.

Downloaded on 2014-04-24 to IP 140.113.38.11 address. Redistribution subject to ECS terms of use (see ecsdl.org/site/terms_use) unless CC License in place (see abstract).

The optical, structural, and electrical properties of the ZnO films were characterized in this work. The crystallinity of the ZnO thin films was investigated by using grazing incidence X-ray diffraction (GIXRD). The thickness of the film was determined by scanning electron microscopy (SEM). Optical transmittance through the sample of ZnO/glass was measured in the wavelength range from 300nm to 800nm by using a UV-VIS-NIR spectrophotometer. Device characteristics, including transfer and output curves, were measured by semiconductor parameter analyzer (HP4156C).

Results and discussion

Effect of different Carrier gases

Figure 3 shows the grazing incident X-ray patterns of 110-nm-thick ZnO films prepared with different carrier gases at a substrate temperature of 100°C by APPJ. From the figure it is seen that ZnO films exhibit hexagonal crystal structure with a preferential growth along (002) plane both in N_2 and CDA samples. The N_2 sample has higher intensity of the (002) plane than CDA, but CDA sample show the higher (100) and (101) peaks than N_2. The may be due to the fact that the gas phase nucleation particle increases when CDA is used as a carrier gas. Since the oxygen is high reactivity, it reacts with precursor in the gas phase leading to the random particle. Nevertheless, the FWHM of (002) peak in N_2 (0.46°) is similar to CDA (0.45°).

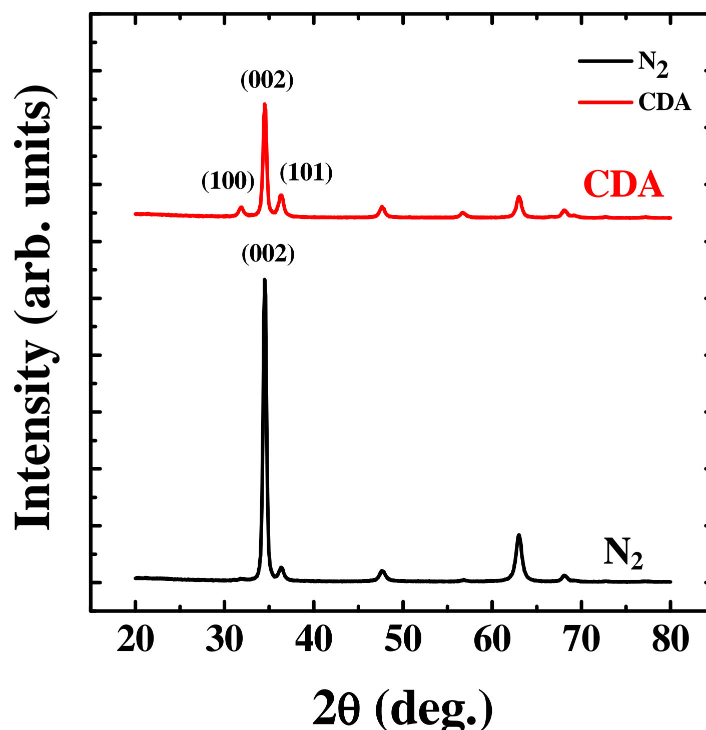

Figure 3 Grazing incident X-ray patterns of ZnO films prepared with different carrier gases.

Downloaded on 2014-04-24 to IP 140.113.38.11 address. Redistribution subject to ECS terms of use (see ecsdl.org/site/terms_use) unless CC License in place (see abstract).

Figure 4 shows the optical transmission spectra of ZnO films deposited on glass with different carrier gases. The average transmittance of N_2 sample is slightly larger than CDA. The possible reason for this may be the scattering light by gas phase nucleation particles. The average optical transmittance of N_2 and CDA samples in the visible range is more than 80%.

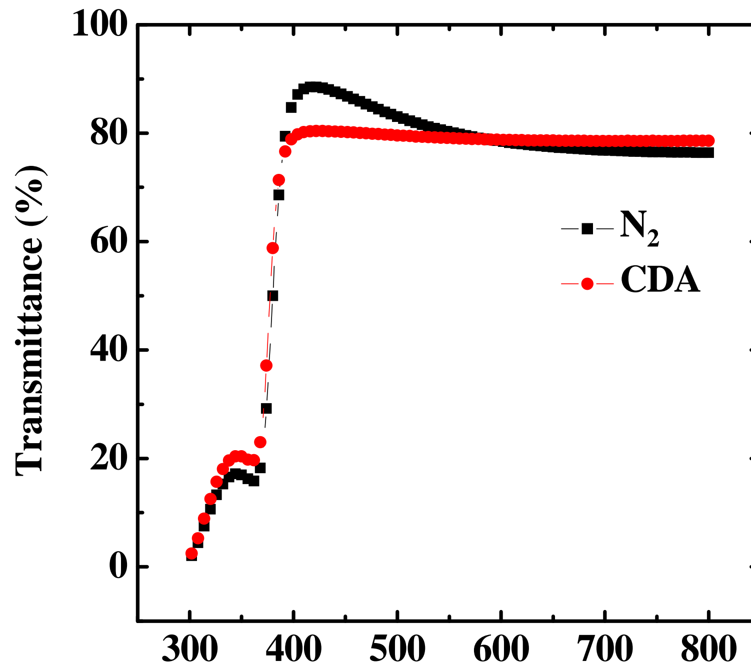

Figure 4 The optical transmission spectra of ZnO films deposited on glass with different carrier gases.

Figure 5 represents transfer characteristics of 110-nm-thick channel ZnO TFTs with different carrier gases. The channel length and width are 100 μm and 1000 μm. From the figure of N_2 sample, it can be observed that high leakage current and the poor Ion/Ioff current ratio. However, ZnO TFT with CDA as carrier gas improves the off-leakage current about 3 orders of magnitude than N_2 sample. It is likely that oxygen species are efficient to repair the oxygen vacancies. The Ion/Ioff ratio of N_2 sample and CDA sample were 1.6×10^2 and 2.59×10^5, respectively. Figure 6 represents $I_{DS}^{1/2}$ versus V_{GS}. The field effect mobility (μ_{FE}) and V_t were extracted using the following current equation.

$$I_D = (W/2L)\, Ci\mu_{FE}\,(V_{GS}-V_t)^2$$

where Ci is the capacitance per unit area of the gate insulator and V_t is the threshold voltage. The μ_{FE} of N_2 sample and CDA sample were 2.3 $cm^2V^{-1}s^{-1}$ $V^{-1}s^{-1}$ and 4.9 cm^2V^{-1} $cm^2V^{-1}s^{-1}$. The CDA sample has lower mobility than N_2. It has been reported that external oxygen was absorbed in the grain boundaries and this oxygen trapped free electrons (7). Although using CDA as a carrier gas repair oxygen vacancies, some adsorbed oxygen in the grain boundaries results in the slight decline of mobility. The threshold voltage of N_2 sample and CDA sample were 16.6 V and 31.5 V respectively, showing that the ZnO-

Downloaded on 2014-04-24 to IP 140.113.38.11 address. Redistribution subject to ECS terms of use (see ecsdl.org/site/terms_use) unless CC License in place (see abstract).

TFT operates the enhancement mode .The result also indicates that CDA sample has the smaller electron carrier concentration than N_2 sample. The background carrier concentration can effectively decrease using CDA as a carrier gas.

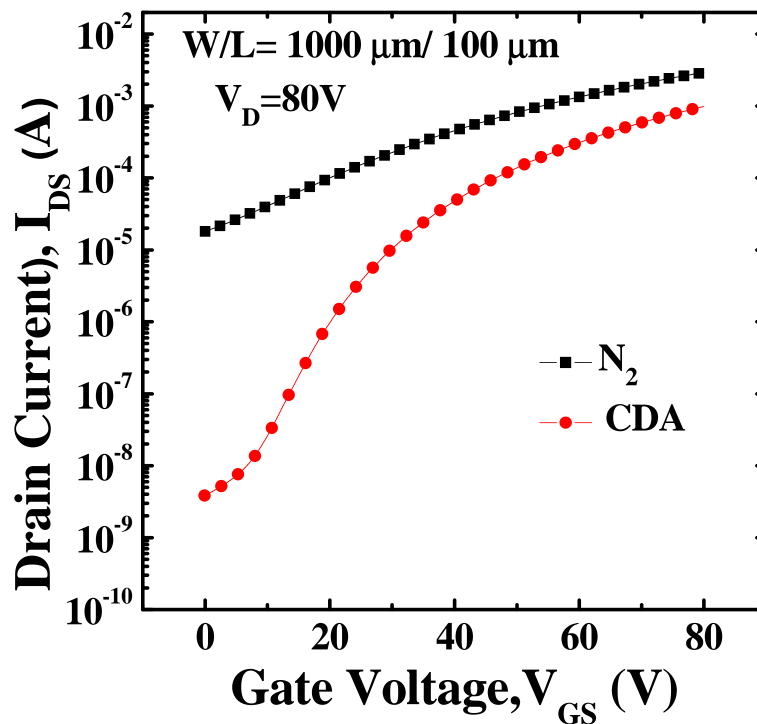

Figure 5 Transfer characteristics of ZnO TFT with different carrier gases.

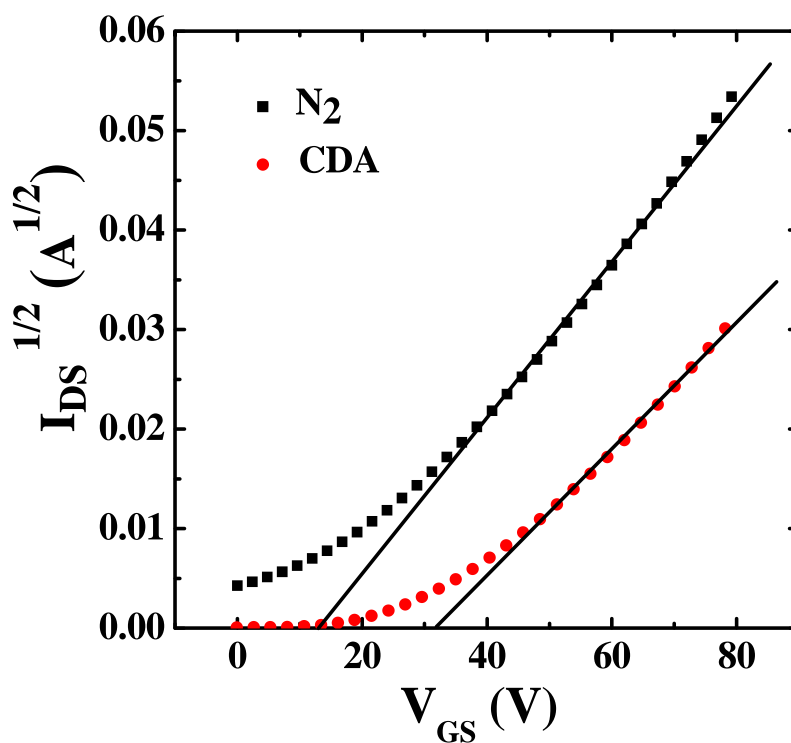

Figure 6 $I_{DS}^{1/2}$ versus V_{GS} at V_D of 80V, used to calculate the threshold voltage and saturation mobility.

Downloaded on 2014-04-24 to IP 140.113.38.11 address. Redistribution subject to ECS terms of use (see ecsdl.org/site/terms_use) unless CC License in place (see abstract).

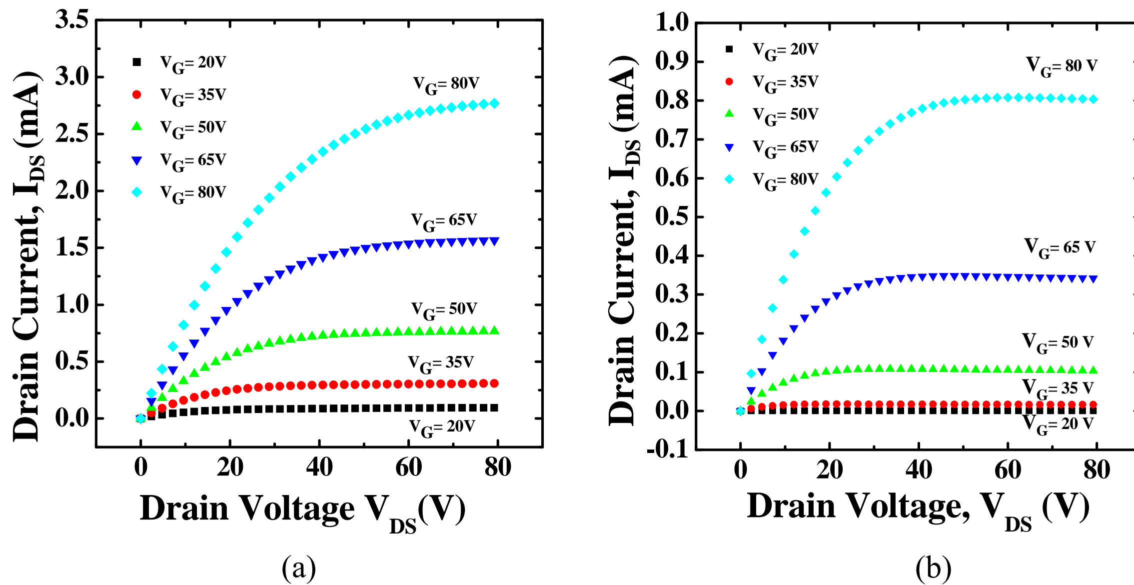

Figure 7 Output characteristics (IDVD) of ZnO TFT with different carrier gas (a) N_2 (b) CDA.

Output characteristics (ID-VD) of ZnO TFT are shown in Figure 7. It is observed that I_D of N_2 sample increase with V_{DS} at saturation region. Since the N_2 sample has higher carrier concentration, the channel region is not totally depleted, and the undepleted region contributes the external current. However, the CDA sample show a hard saturation This indicates that the ZnO channel is fully depletion and this behavior is desired for circuit application because of a lager output resistance (12).

Effect of different channel thicknesses

Transfer characteristics of ZnO TFT with different channel thicknesses are shown in figure 8. The off-leakage current of 110-nm-thick and 165-nm-thick channel ZnO TFTs are 3.82×10^{-9}A and 5.42×10^{-9} A, respectively. The undesired source to drain leakage current flow has less dependence with gate voltage. By reducing the channel thickness, the channel resistance increases result in the low leakage current. When the thickness reduces to 55 nm, the leakage current significantly reduces. The leakage current of 55-nm-thick channel ZnO TFT reaches a minimum value of 3.21×10^{-11} A. Figure 9 shows Output characteristics (IDVD) of ZnO TFT with different channel thicknesses. All the samples operate in enhancement mode, and the 55-nm-thick sample shows a higher saturation current. The mobility of 55 nm sample is higher compared with 110 nm and 165 nm. This may be due to the less series resistance. Table I. summarizes the electrical properties of field effect mobility, threshold voltage, subthreshold swing, and Ion/Ioff ratio with different channel thicknesses. The 55nm-thick ZnO channel layer shows a better performance.

Downloaded on 2014-04-24 to IP 140.113.38.11 address. Redistribution subject to ECS terms of use (see ecsdl.org/site/terms_use) unless CC License in place (see abstract).

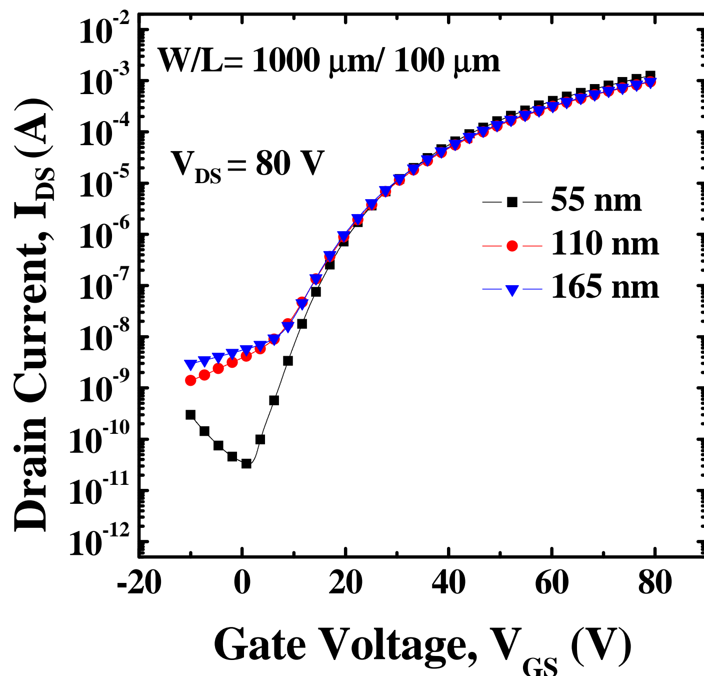

Figure 8 Transfer characteristics of ZnO TFT with different channel thicknesses.

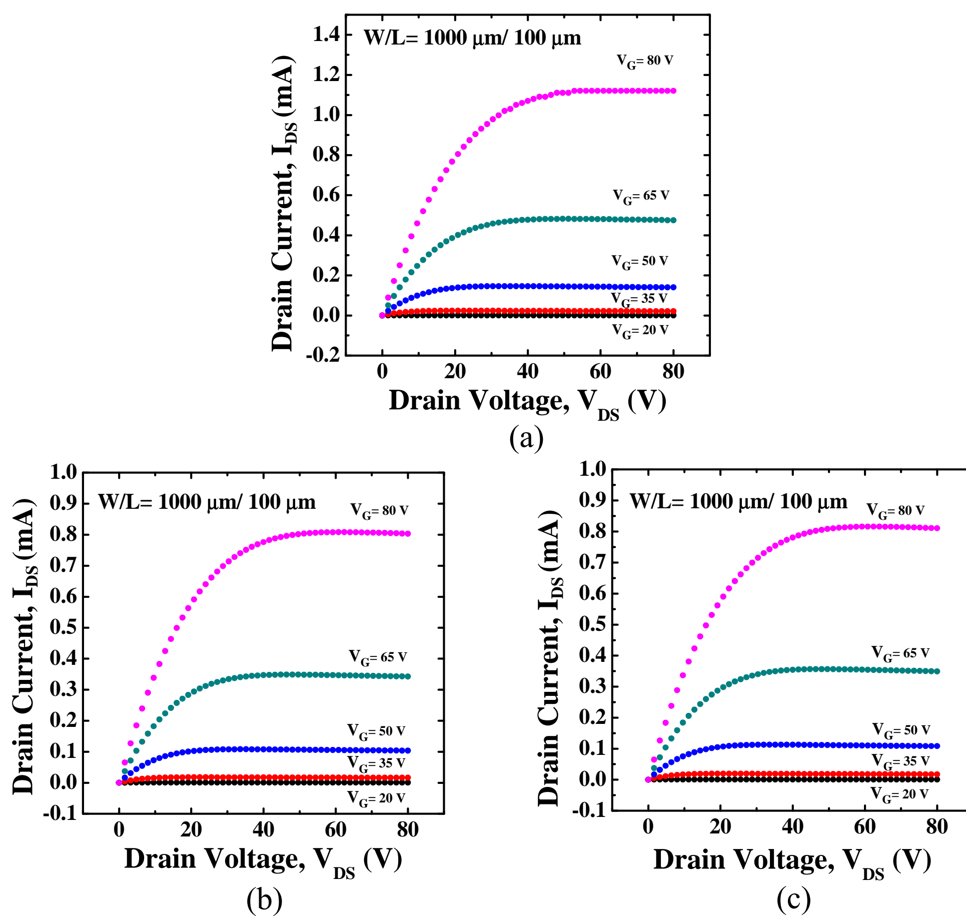

Figure 9 Output characteristics (IDVD) of ZnO TFT with different channel thicknesses (a) 55nm(b) 110nm (c) 165nm.

Downloaded on 2014-04-24 to IP 140.113.38.11 address. Redistribution subject to ECS terms of use (see ecsdl.org/site/terms_use) unless CC License in place (see abstract).

TABLE I.

Channel thickness	Vt (V)	SS (V/dec.)	Mobility ($cm^2/V\text{-}s$)	Ion/Ioff ratio
55 nm	33.8	3.75	3.49	4.08×10^{7}
110 nm	31.5	6.33	2.33	7.06×10^{5}
165 nm	31.1	6.34	2.33	3.34×10^{5}

Conclusion

In summary, ZnO films deposited by APPJ were successfully integrated as a channel layer. The ZnO thin films exhibit a preferred (002) orientation and the average transmittance of ZnO thin films deposited on glass are more than 80%. During deposition, oxygen species can effectively reduce oxygen vacancies and improve the Ion/Ioff current ratio from 1.6×10^{2} to 2.59×10^{5}. Reducing the thickness can increase the channel resistance and reduce the undesired current flow. Using CDA as a carrier gas and reducing the channel thickness to 55nm, a subthreshold swing of 3.75V/decade, a field-effect mobility of 3.49 cm^2/Vs and a Ion/Ioff current ratio of 4.08×10^{7} were obtained.

Acknowledgments

The authors are grateful for the support of this research by the Mechanical and Systems Research Laboratories, Industrial Technology Research Institute (ITRI). The authors would also like to thank the Nano Facility Center (NFC) of National Chiao-Tung University and the National Nano Device Laboratory (NDL) for providing process equipment.

References

1. Z. Fang, X. Xie, J. Li, H. Yang, Y. Qiu and E. Kuffel, *J. Phys. D: Appl. Phys.*, **42**, 085204 (2009).
2. H. Li, S. Wang, L. Zhao and T. Ye, *Plasma Sci. Technol.*, **6**, 2481 (2004).
3. V. Raballand, J. Benedikt and A. von Keudell, *Appl. Phys. Lett.*, **92**, 091502 (2008).
4. Z. Xiaodong, A.-K. Farzaneh, P.-E. Camille and T. Michael, *Plasma Process. Polym.*, **2**, 407 (2005).
5. M. Osada, T. Sakemi and T. Yamamoto, *Thin Solid Films*, **494**, 38 (2006).
6. T. Yoshida, T. Tachibana, T. Maemoto, S. Sasa and M. Inoue, *Applied Physics A: Materials Science & Processing*, **101**, 685.
7. P. F. Carcia, R. S. McLean, M. H. Reilly and J. G. Nunes, *Appl. Phys. Lett.*, **82**, 1117 (2003).
8. J. Jo, H. Choi, J. Yun, H. Kim, O. Seo and B. Lee, *Thin Solid Films*, **517**, 6337 (2009).

Downloaded on 2014-04-24 to IP 140.113.38.11 address. Redistribution subject to ECS terms of use (see ecsdl.org/site/terms_use) unless CC License in place (see abstract).

9. H.-C. Cheng, C.-F. Chen and C.-Y. Tsay, *Appl. Phys. Lett.*, **90**, 012113 (2007).
10. G. Adamopoulos, A. Bashir, P. H. Wobkenberg, D. D. C. Bradley and T. D. Anthopoulos, *Appl. Phys. Lett.*, **95**, 133507 (2009).
11. J. H. Chung, J. Y. Lee, H. S. Kim, N. W. Jang and J. H. Kim, *Thin Solid Films*, **516**, 5597 (2008).
12. E. M. C. Fortunato, P. M. C. Barquinha, A. C. M. B. G. Pimentel, A. M. F. Goncalves, A. J. S. Marques, R. F. P. Martins and L. M. N. Pereira, *Appl. Phys. Lett.*, **85**, 2541 (2004).

Downloaded on 2014-04-24 to IP 140.113.38.11 address. Redistribution subject to ECS terms of use (see ecsdl.org/site/terms_use) unless CC License in place (see abstract).